TISSUE ENGINEERING: Part A
Volume 18, Numbers 21 and 22, 2012

DOI: 10.1089/ten.tea.2011.0479

Development of Microfabricated Dermal Epidermal Regenerative Matrices to Evaluate the Role of Cellular Microenvironments on Epidermal Morphogenesis

Katie A. Bush, Ph.D.,[1,2] and George D. Pins, Ph.D.[2]

Topographic features at the dermal–epidermal junction (DEJ) provide instructive cues critical for modulating keratinocyte functions and enhancing the overall architecture and organization of skin. This interdigitated interface conforms to a series of rete ridges and papillary projections on the dermis that provides three-dimensional (3D) cellular microenvironments as well as structural stability between the dermal and epidermal layers during mechanical loading. The dimensions of these cellular microenvironments exhibit regional differences on the surface of the body, and quantitative histological analyses have shown that localization of highly proliferative keratinocytes also varies, according to the regional geometries of these microenvironments. In this study, we combined photolithography, collagen processing, and biochemical conjugation techniques to create microfabricated dermal epidermal regeneration matrices (μDERMs) with features that mimic the native 3D cellular microenvironment at the DEJ. We used this model system to study the effect of the 3D cellular microenvironment on epithelialization and basal keratinocyte interaction with the microenvironment on the surface of the μDERMs. We found that features closely mimicking those in high-friction areas of the body (deep, narrow channels) epithelialized faster than features mimicking low-friction areas. Additionally, when evaluating β1 expression, an integrin involved in epidermal morphogenesis, it was found that integrin-bright expression was localized in the depths of the features, suggesting that the μDERMs may play a role in defining cellular microenvironments as well as a protective environment for the regenerative population of keratinocytes. The outcomes of this study suggest that μDERMs can serve as a robust biomimetic model system to evaluate the roles of the 3D microenvironment on enhancing the regenerative capacity and structural stability of bioengineered skin substitutes.

Introduction

Bioengineered skin substitutes were the first functional engineered tissues to be made commercially available.[1–5] While clinical studies have shown that bioengineered skin substitutes can restore damaged skin, many limitations still exist, including the time to achieve definitive wound closure, the generative capacity of the bioengineered skin substitute, contracture of the wound site leading to scarring, and mechanically induced epithelial shearing or graft failure.[6–11] A common design feature to current bioengineered skin substitutes is a flat interface at the dermal–epidermal junction (DEJ). In native skin, the DEJ is not flat, but rather conforms to a series of three-dimensional (3D) rete ridges and papillary projections of the dermis, ranging 50–400 μm in width and 50–200 μm in depth, which provide structural integrity to the skin and defines the cellular microenvironments, critical for the proper functioning of the basal and suprabasal keratinocytes located in these regions.[12,13]

The 3D cellular microenvironments or microniches at the DEJ correlate with the spatial organization of keratinocyte markers for proliferation and terminal differentiation. Basal keratinocytes adhere at the DEJ through β_1 integrins, which are involved in regulating stratification and the initiation of terminal differentiation.[14–20] Basal keratinocytes with the highest proliferation potential express higher levels of β_1 than other basal keratinocytes.[21–23] Studies have shown that basal keratinocytes with increased levels of β_1 integrin expression are localized in regions of the microenvironment, depending on the body location. Areas of the body that are subject to excess shear stress or friction, such as the palms of the hands and the soles of the feet, contain numerous narrow and deep rete ridges, and β_1 integrins are localized to the deepest portion of their microenvironments. In areas that are subject to less friction, such as the breast, scalp, and foreskin, the microenvironmental features at the DEJ are wider and shallower than high-friction areas, and β1 integrin expression is localized to the tip of the papillary projections.[22,24,25]

[1]Program in Biomedical Engineering and Medical Physics, University of Massachusetts Medical School, Worcester, Massachusetts.
[2]Department of Biomedical Engineering, Worcester Polytechnic Institute, Worcester, Massachusetts.

Understanding how the structural cues of the cellular microenvironments modulate keratinocyte functions through cell–cell adhesions and extracellular matrix protein adhesions as well as enhancing the overall architecture, organization, and mechanical stability of the tissue is a critical component for enhancing the performance of bioengineered skin substitutes. In this study, we used photolithography to create microfabricated dermal epidermal regeneration matrices (μDERMs) with features mimicking the native topographical microenvironments or microniches at the DEJ to study the effect of physical features on basal keratinocyte functions. The morphology of the formed epidermis, the thickness of the epithelial layer, proliferation, and localization of β1 integrin were evaluated to determine the effects of the 3D microenvironments in creating a robust bioengineered skin substitute.

Materials and Methods

Production of μDERMs

To mimic the microtopography found at the DEJ, photolithography was used to create a master silicon wafer.[26] To create negative replicate molds, a polydimethylsiloxane silicone elastomer (PDMS, Sylgard 184; Dow Corning Corp.) was poured onto the surface of the wafer (10:1 base to curing agent), degassed to remove trapped air bubbles, and allowed to polymerize. The PDMS was then carefully separated from the silicon wafer (Fig. 1).

Acid-soluble type I collagen (CI) was extracted from rat tail tendons, which were received from animals euthanized for other protocols (approved by the Worcester Polytechnic Institute, Worcester, MA and Institutional Animal Care and Use Committee).[27,28] The CI was lyophilized and resuspended at a concentration of 10 mg/mL in 5 mM HCl (Sigma Aldrich). The CI solution was then self-assembled using 5×Dulbecco's modified Eagle's medium (DMEM; Invitrogen) with 0.22 M $NaHCO_3$ and 0.1 M NaOH (Sigma) and incubated at 37°C for 18 h on circular negative replicated PDMS molds to create the microfabricated portion of the μDERMs (Fig. 1C).[29]

A collagen–glycosaminoglycan (GAG) coprecipitate containing collagen (5 mg/mL) and GAG (0.18 mg/mL) was prepared.[30] The collagen–GAG coprecipitate was placed into an aluminum weigh boat, lyophilized, and crosslinked using thermal dehydration at 105°C in a vacuum of <200 mtorr for 48 h. The collagen–GAG sponges were cut into rectangles approximately 7 cm^2 (2.5-cm width×3-cm length) and placed in a desiccator until use.

After self-assembly of the microfabricated portion of the μDERM was complete, a small volume (200 μL) of 10 mg/mL solution of CI was neutralized using 5×DMEM containing 0.22 M $NaHCO_3$ and placed directly on the back of the microfabricated portion of the μDERM. This glue was gently spread to cover the entire surface area. Immediately following this step, a precut collagen–GAG sponge was placed on top of the neutralizing CI and incubated at 37°C for 2 h to facilitate complete self-assembly of the CI and lamination of the two components (Fig. 1D). Carbodiimide 1-ethyl-3-(3-dimethylaminopropyl) carbodiimide hydrochloride (EDC; Sigma) at a mole ratio of 5:1 EDC to carboxylic acid groups in CI was used to covalently conjugate fibronectin (FN) to the μDERM surface and to crosslink the μDERM.[29,31] The μDERMs were removed from the EDC solution and immediately placed into air/liquid (A/L) interface culture devices,[29] and FN (BD Biosciences, Bedford, MA) at 100 μg/mL was conjugated to the surface of the μDERM overnight at room temperature (Fig. 1F). Control μDERMs without FN conjugation were also prepared. These controls received EDC and dPBS instead of FN.

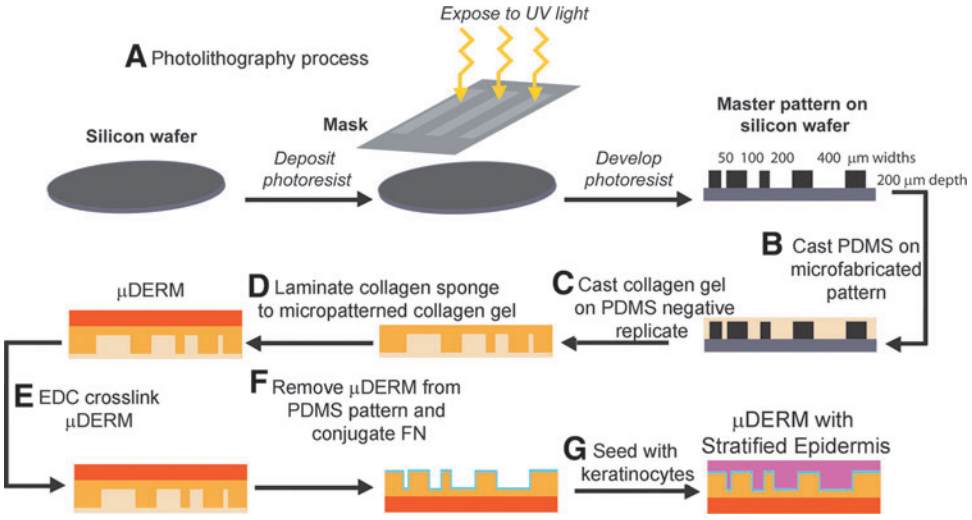

FIG. 1. Production of microfabricated dermal epidermal regenerative matrices (μDERMs) **(A)**. Photolithography was used to create a master pattern on a silicon wafer containing channels with a depth of 200 μm and widths of 50, 100, 200, and 400 μm. Polydimethylsiloxane (PDMS) was cast on the microfabricated silicon wafer **(B)** and allowed to polymerize. The PDMS pattern was inverted, and a collagen gel was cast onto the surface containing the negative replicate of the original pattern **(C)**. Once polymerized, another collagen gel was cast onto the back surface of the original collagen gel to laminate a collagen–glycosaminoglycan sponge **(D)**, creating a μDERM. The μDERM was then EDC crosslinked **(E)** and removed from the PDMS. Fibronectin (FN) was then conjugated to the microfabricated surface of the μDERM **(F)**. The μDERM was sterilized, seeded with keratinocytes **(G)**, and cultured. Color images available online at www.liebertpub.com/tea

Culture of μDERMs

Neonatal keratinocytes (NHKs) were cultured as previously described.[30,32] Neonatal foreskins were obtained from nonidentifiable discarded tissues from the UMass Memorial Medical Center, Worcester, MA, and were approved with an exempt status from the New England Institutional Review Board. After 5 days of culture, NHKs were detached using 0.05% Trypsin–EDTA (Invitrogen), and passage 2–3 NHKs from multiple donors were used in all experiments.

The μDERMs were sterilized using 70% ethanol and excessive sterile water rinses, and then were preconditioned with a seeding medium consisting of a 3:1 mixture of 1×DMEM (high glucose) and Ham's F-12 medium supplemented with 10^{-10} M cholera toxin, 0.2 μg/mL hydrocortisone (Calbiochem), 5 μg/mL insulin, 50 μg/mL ascorbic acid (Sigma), and 100 IU/mL and 100 μg/mL penicillin–streptomycin. Keratinocytes were seeded using this medium at 500,000 cells/cm^2 and allowed to adhere for 2 h in 10% CO_2 at 37°C. After 2 h, the seeding medium containing 1% fetal bovine serum (FBS) was placed in each well, completely submerging the μDERMs. After 24 h, the NHK seeding medium was removed, and the μDERMs were submerged for an additional 48 h in an NHK priming medium composed of an NHK seeding medium (with FBS) supplemented with 24 μM bovine serum albumin (BSA), 1.0 mM L-serine (Sigma), 10 μM L-carnitine (Sigma), and a mixture of fatty acids, including 25 μM oleic acid (Sigma), 15 μM linoleic acid (Sigma), 7 μM arachidonic acid (Sigma), and 25 μM palmitic acid (Sigma).[33] After 48 h in a priming medium, the μDERMs were cultured for 3 or 7 days with an A/L interface medium composed of a serum-free NHK priming medium supplemented with 1.0 ng/mL EGF (Fig. 1G). As controls, μDERMs without FN treatment and decellularized dermis (DED) were cultured in parallel using the same process; however, DED was not sterilized, but placed directly into sterile A/L interface culture devices, and NHKs were seeded on the papillary surface. Previous immunohistochemical analyses demonstrated that DED, prepared using rapid freeze–thaw cycles described previously, retains key proteins of the basal lamina, including laminin, collagen IV, and collagen VII.[40]

Quantitative morphometric analysis of μDERMs

To measure the surface features of the μDERMs, a series of unseeded μDERMs were embedded in Paraplast (McCormick Scientific) and sectioned in a plane perpendicular to the surface of the basal lamina. Slides were hematoxylin and eosin (Richard Allen Scientific) stained. For each sample, the depths of the channels and the widths of the channels were measured using ImageJ software (Fig. 2A) (downloaded from http://rsb.info.nih.gov). Values are reported as mean±SEM.

Epidermal thickness and graft morphology

Epidermal thickness and graft morphology of the μDERMs were evaluated after 3 or 7 days of A/L interface culture using hematoxylin and eosin. Measurements of the channel depth, channel widths, and epithelial thickness in each channel were made. Additionally, the epidermal thickness of the flat region adjacent to the channels (papillary plateau) was measured. For each μDERM, multiple

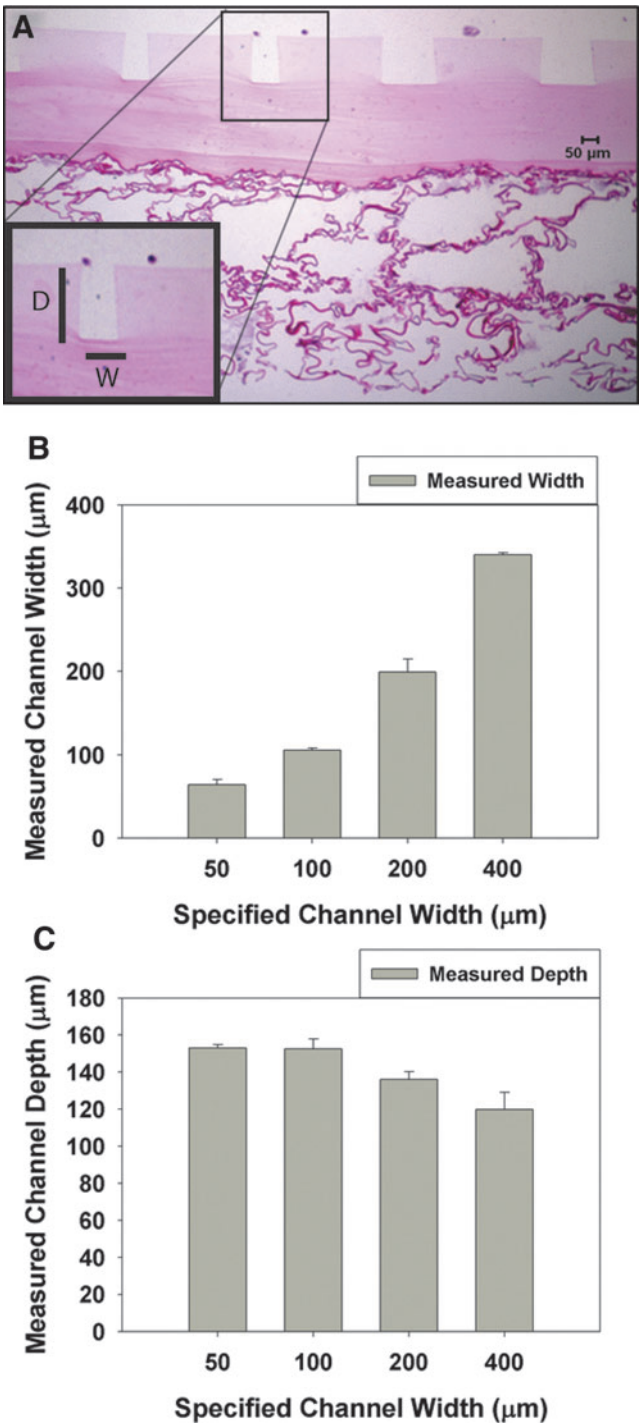

FIG. 2. Topographical measurements of the surfaces of μDERMs. The topography of the μDERMs was measured using histological sections and quantitative image analysis. **(A)** μDERM section stained with eosin. The insert illustrates the measurements made for depths (D) and widths (W) of the channels. These values were averaged and plotted in **(B)** (width) and in **(C)** (depth) against specified channel widths. Values are reported as averages±SEM. $n=4$ for 50-μm channels, and $n=5$ for 100-, 200-, and 400-μm channels. Color images available online at www.liebertpub.com/tea

measurements were made, since each μDERM contained multiple channels. For epithelialized DED and native tissues, the thickness of the epidermal layer was measured in the rete ridges and on the papillary plateaus. The dimensions of the rete ridges were also measured.

To characterize the effect of channel dimensions on the epidermal thickness, the epidermal thicknesses were measured in channels with widths that were within ± 2 SEM of the topography validation width measurements, for each specified channel width. Data points were excluded from all other channels from this analysis. These data points were then individually normalized to the depth of their channel. The normalized data from each specified channel width were then averaged and reported as a mean value ± SEM. Sample values for the 50-, 100-, 200-, and 400-μm-width channels were $n = 5$, 5, 6, and 11 at 3 days, respectively, and $n = 5$, 6, 15, and 13 at 7 days, respectively. At both 3 and 7 days, $n = 4$ for DED, and $n = 4$ for foreskin tissue.

Keratinocyte proliferation

Proliferation of basal NHKs was evaluated after 3 or 7 days of A/L interface culture by measuring the presence of Ki67, a cell cycle-associated antigen. A prediluted mouse anti-human Ki67 antibody (Zymed Laboratories) was used in conjunction with biotinylated anti-mouse IgG (Vector Laboratories, Inc.) at 1:200. The Vectastain Elite ABC Kit (Vector Laboratories) and Vector NovaRED Substrate Kit were then used to detect positive expression of the antibody. The number of Ki67-positive basal cells and the total basal cell number were counted over the length of the basal lamina in each channel and for control tissues, over the entire image. The data from each specified channel width were averaged and reported as the mean value ± SEM. Samples for 50-, 100-, 200-, and 400-μm-width channels were $n = 5$, 6, 7, and 10 at 3 days, respectively, and $n = 5$, 6, 10, and 11 at 7 days, respectively. At both 3 and 7 days of A/L interface culture, $n = 4$ for epithelialized DED. Samples for foreskin tissue were $n = 5$. Only one sample of breast control tissue was obtained, and three images of the sample were evaluated and reported as the mean ± standard deviations. Breast tissue was not included in statistical analyses. Human foreskins and breast tissue were obtained from nonidentifiable discarded tissues from the UMass Memorial Medical Center, Worcester, MA, and were exempt from the New England Institutional Review Board review.

β_1 integrin expression

The expression of β_1 integrin for basal NHKs was evaluated on μDERMs, epithelialized DED, and human tissues, using immunohistochemistry. Anti-CD29 (BioGenex) was applied at a concentration of 1:100, and goat anti-mouse (Alexa Fluor 546; Invitrogen) secondary antibody was used at a dilution of 1:100. After secondary antibody incubation, the sections were rinsed, and Hoechst nuclear reagent (Invitrogen) was added at 0.06 mM. Each section was imaged using the same exposure time, and the images were analyzed using ImageJ software. Following previously published methods, the greatest fluorescence intensity recorded was subdivided into three regions, the dullest (bottom 1/3), the brightest (top 1/3), and the remaining (middle 1/3). Cells that had intensity values in the top 1/3 around their perimeter were considered integrin-bright.[21,22,34] The number of cells that were integrin-bright was counted as well as the total number of basal cells.

Statistical analyses

Sigma Stat Version 3.10 (Systat Software, Inc.) was used to evaluate statistical differences. To determine if the means of two different samples were significantly different, either a Student's *t*-test or the Mann–Whitney Rank Sum Test was used, depending on if the samples were drawn from a normally distributed population with equal variance. For both the Student's *t*-test and the Mann–Whitney Rank Sum Test, a p-value < 0.05 indicated a significant difference between the means of experimental groups. To determine statistical differences among the means of three or more experimental groups, a One-Way Analysis of Variance (ANOVA) was used when the samples were drawn from a normally distributed population with equal variance. When the data were not normally distributed, a Kruskal–Wallis One-Way ANOVA on ranks was performed. When a statistical difference was detected among the group means, a Turkey *posthoc* analysis was performed for both the One-Way ANOVA and Kruskal–Wallis One-Way ANOVA on ranks. A p-value < 0.05, for both variance tests, indicated a significant difference between the groups.

Results

Development of μDERMs

To investigate the role of the cellular microenvironments on epithelialization and the regenerative capacity of bioengineered skin substitutes, we developed a process to create a dermal scaffold with defined topographical features. The topographical features of μDERMs were analyzed using quantitative morphometric analyses of histological sections before cell seeding. Depths and widths of the channels were measured (Fig. 2). The widths for each channel were measured (Fig. 2B) and found to be 60.8 ± 3.8 for the 50-μm-width channels, 101.2 ± 2.4 for the 100-μm channels, 197.1 ± 13.5 for the 200-μm channels, and 315.7 ± 27.9 for the 400-μm-width channels. The depth for each channel was also measured and found to be approximately 150 μm (Fig. 2C).

Epidermal thickness and graft morphology are influenced by μDERM features

The effect of the cellular microenvironments on epidermal thickness was analyzed at 3 or 7 days of A/L interface culture on μDERMs. Surfaces conjugated with FN (Fig. 3C, D) had continuous, stratified layers of cells, regardless of topographical geometry, whereas control surfaces without FN conjugation did not (Fig. 3A, B). When comparing grafts cultured with FN at various time points, the geometric features influenced the thickness of the epidermal layer that formed on the surfaces of the skin substitutes. At 3 days of A/L interface culture, channels with widths of 50 μm had noticeably thicker epidermal layers than channels with widths of 200 μm (Fig. 3C, D, respectively). Epidermal thickness normalized to the depth of the channel at 3 days of A/L interface culture for the 50 μm channels was statistically greater than the thickness measured for the 100-μm-width, 200-μm-width, and 400-μm-width channels (Fig. 4).

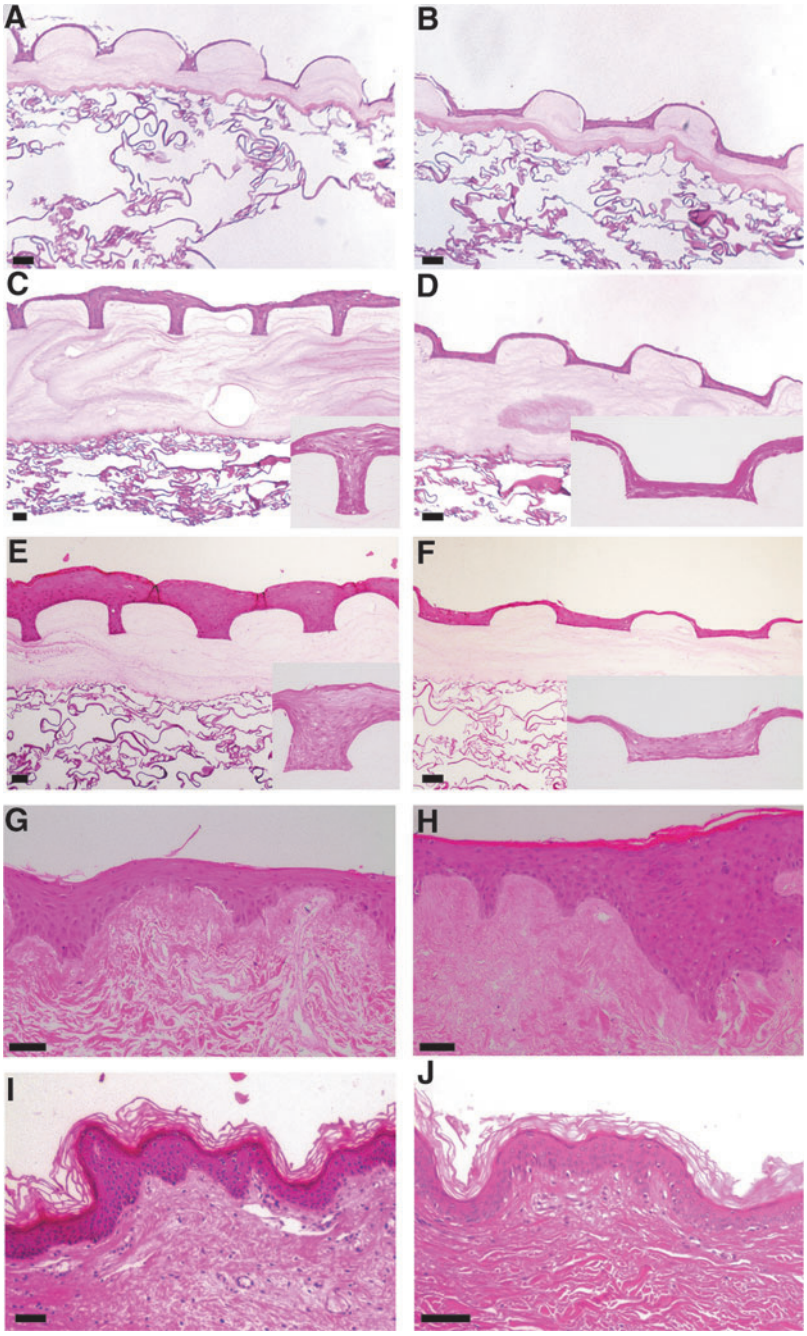

FIG. 3. Hematoxylin and eosin staining of μDERMs and control tissues. To evaluate the effects of FN and topography on epithelialization, the epidermal thickness was measured on μDERMs without FN cultured for 3 days at the air/liquid (A/L) interface **(A** and **B**, respectively**)**, μDERMs with FN cultured for 3 days at the A/L interface **(C** and **D**, respectively**)**, and 7 days at the A/L interface **(E** and **F)** and compared to keratinocytes cultured on decellularized dermis (DED) cultured for 3 or 7 days at the A/L interface **(G** and **H**, respectively**)** as well as foreskin and breast control tissues **(I** and **J**, respectively**)**. Scale bars = 50 μm. Color images available online at www.liebertpub.com/tea

The epidermal layer on the μDERMs in the 50-μm-width channels was similar in the thickness and morphology to the epidermal layer cultured on DED for 3 days at the A/L interface (Fig. 3G). When quantifying epidermal thicknesses, no statistical differences were found between the DED and the 50-μm-width channels at 3 days (Fig. 4). At the 7-day A/L interface culture time point for μDERMs, the 50-μm-width and 100-μm-width channels (Fig. 3E) had similar morphologies and epidermal thicknesses, and both channels had notably thicker epidermal layers than comparable 200-μm-width channels (Fig. 3F).

Epidermal thicknesses for the 50-μm-width and 100-μm-width channels had similar values, and were both statistically different from the 200-μm-width and 400-μm-width channels at day 7 (Fig. 4). When comparing the epidermal layers on μDERMs at 7 days of A/L interface culture with DED (Fig. 3H) and native foreskin and breast skin (Fig. 3I, J, respectively), we observed that the 50-μm- and 100-μm-width channels have similar morphologies and thicknesses. No statistical differences were found in epidermal thickness between 50-μm-width and 100-μm-width channels at 3 days. Additionally, no statistical differences were found in epidermal thickness between 50-μm-width and 100-μm-width channels and the epidermal thickness of cells cultured for 7 days at A/L interface on DED or foreskin tissue (Fig. 4).

To compare epidermal thicknesses achieved independent of the channel depth or the rete ridge height, we measured the epidermal thicknesses on flat, control surfaces, the

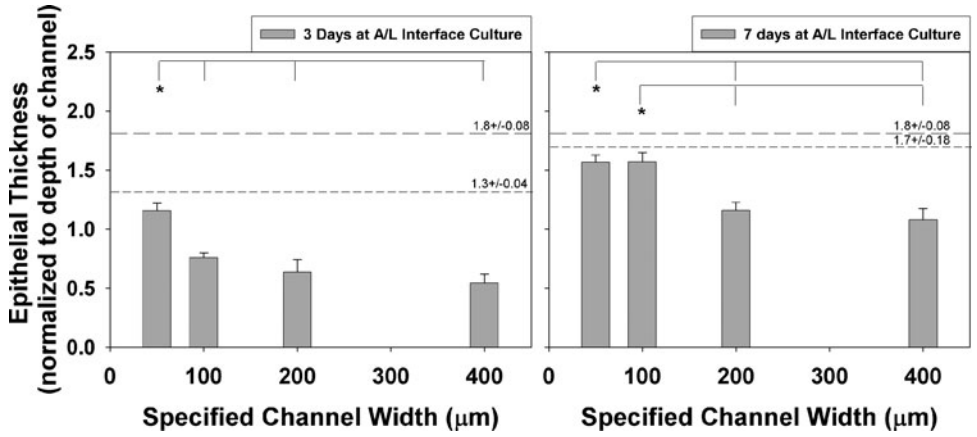

FIG. 4. Epithelial thickness measured and normalized to depth of channel. Epithelial thickness was measured in each channel of each μDERM and normalized to the depth of the channel. * indicates $p < 0.05$, one-way analysis of variance (ANOVA), Turkey *post-hoc* analysis. The large dashed lines represent epithelial thickness of foreskin tissue, and the smaller dashed lines represent epithelial thickness on DED. Values are averages ± SEM. $n = 5$ for both 50- and 100-μm channels at 3 and 7 days; $n = 6$ and 15 for 200-μm channels at 3 and 7 days, respectively, and $n = 11$ and 13 for 400-μm channels at 3 and 7 days, respectively.

papillary plateaus of the μDERMs. The epidermal thicknesses on papillary plateaus between all channels were averaged and compared to thicknesses on the papillary projections for epithelialized DED and foreskin tissue. At 3 days of A/L interface culture, μDERMs and epithelialized DED were not statistically different from each other, but different from native foreskin. At 7 days of A/L interface culture, the epidermal thicknesses at the papillary plateau were not statistically different between any measured tissues (Fig. 5).

Basal keratinocyte proliferation capacity on μDERMs is affected by microenvironmental features

The effects of microtopography on cell proliferation were evaluated after 3 or 7 days of A/L interface culture. Foreskin and breast tissues were also evaluated as native skin controls (Fig. 6). At 3 and 7 days of A/L interface culture, the 50-μm-width channels had a low average percentage of Ki67-positive cells (Fig. 7), with 40% of the channels having zero Ki67-positive cells. When analyzing the 100-μm-width channels after 3 days of A/L interface culture, a similar percentage of Ki67 cells was found as in the 50-μm-width channels. At 7 days of A/L interface culture for the 100-μm-width channels, the percentage of Ki67-positive cells increased (Fig. 7).

The 200-μm-width and 400-μm-width channels had similar values and trends at both 3 and 7 days of A/L interface culture with values statistically decreasing from day 3 to day 7 (Student's *t*-test, $p < 0.05$). Epithelialized DED exhibited an increase in percentage of Ki67-positive cells from day 3 to day 7, similar to the 100-μm-width channels. When analyzing native tissue controls, the basal keratinocytes of neonatal foreskin were approximately 20% Ki67 positive, and basal keratinocytes in breast tissue were approximately 10% Ki67 positive.

Microenvironments of μDERMs control spatial localization of β_1-integrin-bright basal NHKs

To determine localization of β_1-bright NHKs on μDERMs, epithelialized DEDs, and native foreskins, we utilized immunohistochemistry, coupled with quantitative digital image analyses. Fluorescent intensity values were determined for cell–cell borders similar to previously reported literature for 3-day A/L interface cultures.[21,22,34] Native foreskin tissue displayed β_1-bright regions on the tips of the papillary projections (Fig. 8A–C). On the μDERMs, β_1-bright regions were located in the channels. Analyses indicated that for the 100-

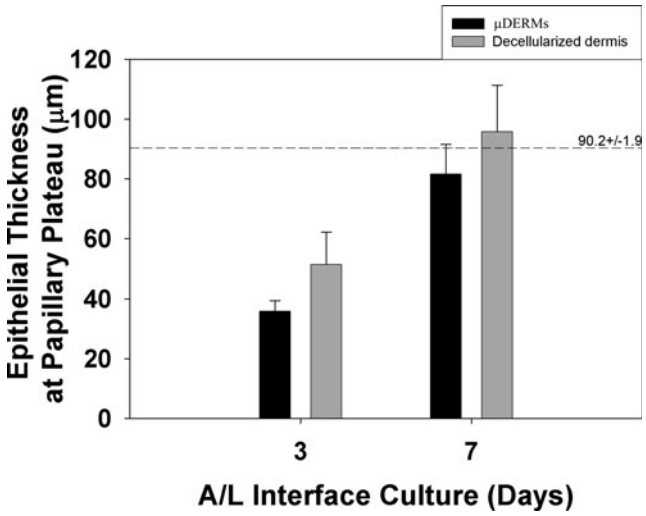

FIG. 5. Epithelial thickness at the papillary plateau. The thicknesses of the epidermal layers at the papillary plateaus of μDERMs, at the epithelialized DED, and in native foreskin were measured. No statistical differences were detected between the thicknesses of μDERMs and epithelialized DED at 3 or 7 days of A/L interface culture (One-Way ANOVA with Turkey *post-hoc* analysis). At 7 days, there were no statistical differences between foreskin tissue and either the μDERMs or epithelialized DED (Kruskal–Wallis One-Way ANOVA on Ranks). Values are averages ± SEM. $n = 14$ and 15 for μDERMs at 3 and 7 days, respectively, $n = 4$ and 7 for decellularized dermis at 3 and 7 days, respectively, and $n = 4$ for foreskin tissues.

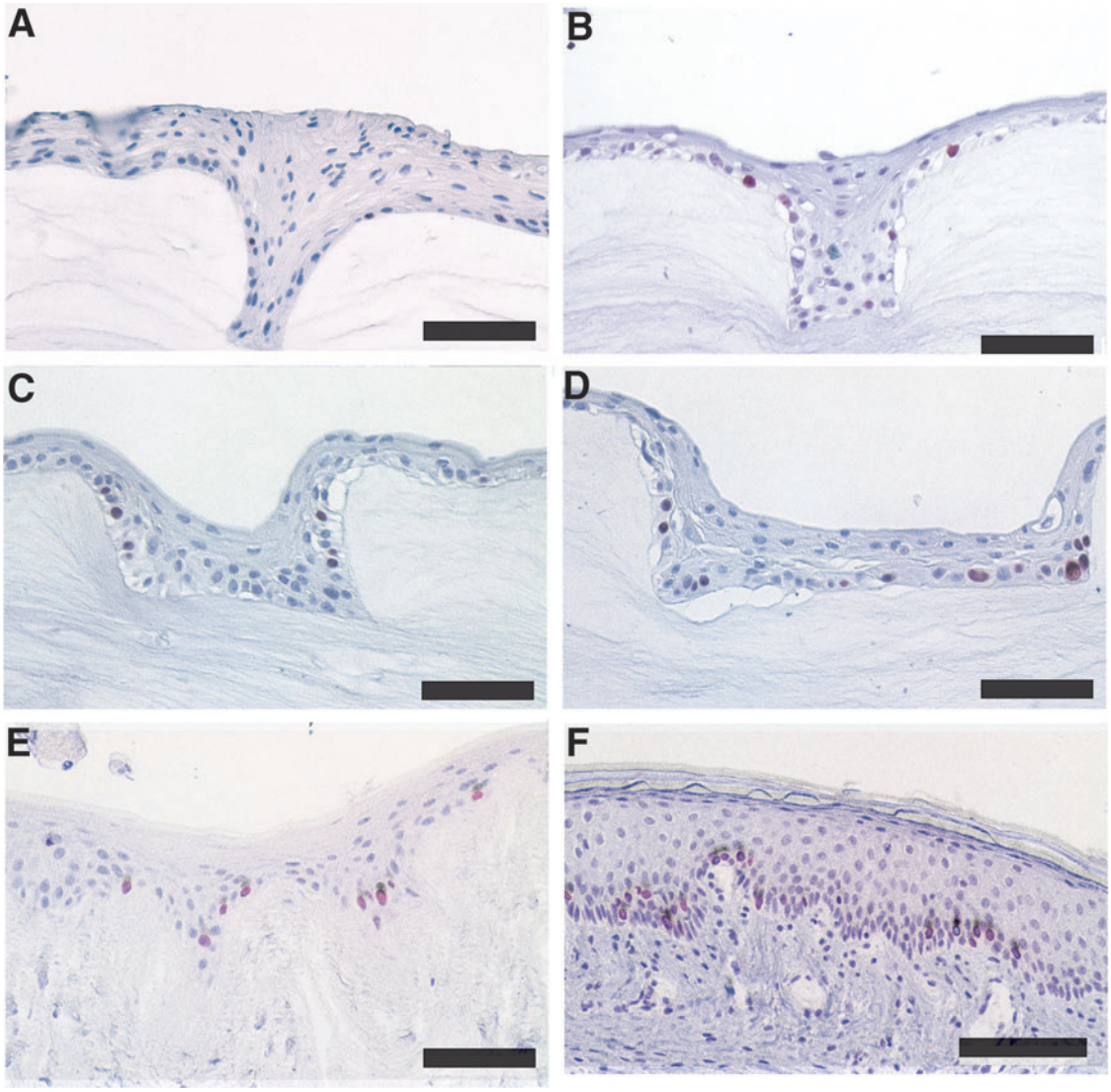

FIG. 6. Histological representation of Ki67 expression of basal keratinocytes present on μDERMs and control tissues. To evaluate the effects of topography on the presence of proliferating basal keratinocytes, Ki67, a marker for highly mitotic cells, was used. The presence of Ki67-positive basal keratinocytes was evaluated on μDERMs **(A–D)** cultured at 3 days at the A/L interface. **(A)** represents channels with 50-μm widths; **(B)** represents channels with 100-μm widths; **(C)** represents channels with 200-μm widths, and **(D)** represents channels with 400-μm widths. The presence of Ki67-positive cells was also evaluated on keratinocytes cultured on DED for 3 days at the A/L interface **(E)** and to foreskin tissue **(F)**. Scale bars in all images = 100 μm. Color images available online at www.liebertpub.com/tea

μm-width channel (Fig. 8D, E, solid lines in 8E separates flat from channel regions), 16.7% of the total basal keratinocyte population in the channel were β_1-bright. Similar analysis for the 400-μm-width channel indicated that 23% of the total basal keratinocyte population in the channel were β_1-bright (Fig. 8F, G, solid lines in 8G separates flat from channel regions). Additionally, it was found that the β_1-bright regions in the 400-μm-width channels localized to the corners of the channels as seen in Figure 8H and I. When evaluating the corner regions of the 400-μm-width channels (Fig. 8H, I), 50% of the basal keratinocytes were β_1-bright. When flat regions of the μDERMs were evaluated (Fig. 8J, K), β_1-bright cells were heterogeneously dispersed, and 30% of the total basal keratinocyte population were β_1 bright. For epithelialized DED (Fig. 8L, M), 15.6% of the total basal keratinocyte population were β_1-bright, and these cells were localized to the rete ridges. In native foreskin tissue (Fig. 8A, B, C), 7% of the total population of basal keratinocytes were β_1-bright, and these cells were localized to the tips of the dermal papillae. This localization finding is consistent with literature, although our percentage of integrin bright cells was much lower.[21,22] This outcome may be caused by a variation in the fluorescence intensities that the samples were exposed to in this study. Care was taken to not overexpose the regions; thus, lower percentages of bright cells could be caused by this factor.

Discussion

The 3D microenvironment at the DEJ creates a cellular microenvironment that modulates keratinocyte functions through cell–cell and cell–extracellular matrix protein

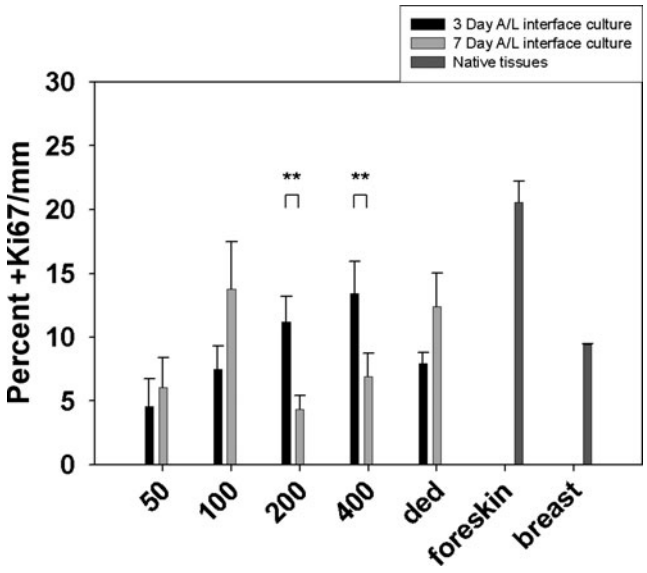

FIG. 7. Quantification of percent positive Ki67 cells/mm on μDERMs and in native tissues. The percentage of Ki67-positive cells was counted over the length of the μDERMs. For channels, the μDERM length was the perimeter of the channel, which was approximately 350, 400, 500, and 700 μm for 50-, 100-, 200-, and 400-μm channels, respectively. For tissues, the length ranged between 650 and 900 μm based on the native topography of the basal lamina. Values are reported as averages ± SEM. $n = 5$, 6, 7, 11, and 4 for 50, 100, 200, 400 μm, and DED at 3 days, respectively; $n = 4$, 5, 11, 10, and 4 for 50, 100, 200, 400 μm, and DED at 7 days, respectively. $n = 5$ for foreskin tissue. ** indicates significant differences, $p < 0.05$, student's *t*-test.

adhesions and proximal autocrine and paracrine cellular signaling factors. Additionally, this topography is critical in maintaining the structural integrity of skin. To date, there is no bioengineered skin substitute that contains the 3D microenvironment located at the DEJ, and the papillary projections and rete ridges must form *de novo* after transplantation. The formation of papillary projections and rete ridges between epidermal and dermal components has been reported after transplantation of composite bioengineered skin substitutes; however, formation does not always occur, and when it has been reported, inconsistencies in the time of formation and the size of rete ridges exist.[35–39] Furthermore, bioengineered skin substitutes lacking the 3D microenvironment at the DEJ have been reported to be fragile and prone to accidental separation of epithelial and dermal components during handling.[40] In this study, we developed a μDERM that contains the 3D microenvironment found at the DEJ and evaluated the role of the native microenvironment in guiding the integration of transplanted cells and their derivatives into a functional tissue equivalent.

The morphology of the epidermal layer on the FN-conjugated μDERMs suggests well-differentiated epidermal layers based on the cellular size and loss of nuclei from the stratum corneum layer. Keratinocytes found in the basal layer are cuboidal in shape, and as the cells progress to the stratum corneum, they exhibit a more flattened morphology. In native skin, these morphological changes are accompanied by changes in the expression of keratin proteins and waterproofing lipids, which significantly enhance skin function by providing both a protective barrier against the environment as well as structural integrity of the epidermis.[41]

The data obtained from the proliferation marker study (Ki67) help to elucidate the trends from the epithelial thickness experiments and suggest that a space-filling mechanism can explain why epithelialization occurs more rapidly for the narrow-width channels than the wider channels. The data suggest that after initial seeding, a proliferative burst occurred, similar to results seen during *in vitro* cultures of low-density to high-density keratinocytes,[42–45] as well as in the *in vivo* wound-healing environment once a monolayer of keratinocytes is formed and contact inhibition occurs.[46] This burst can be characterized by the basal cells undergoing two to four mitotic divisions and committing to terminal differentiation that leads to epithelialization.[44,45,47] Since the 50-μm-width channels have much smaller dimensions, they require fewer cells to fill the topographic feature, followed by the 100-, 200-, and 400-μm-width channels. At 3 days of A/L interface culture (6 days of total culture), the 50-μm-width channels had a complete epithelial layer; however, the 100-, 200-, and 400-μm-width channels did not. The Ki67 data suggest that a proliferative burst occurred before the 3-day time point, and this channel was in a steady state of proliferation at the 3-day and 7-day time points, whereas the other channels were still undergoing a proliferative burst to fill the channel. At 7 days of A/L interface culture (10 days of culture), the 100-μm-width channels had the same epithelial thickness as the 50-μm-width channels and native skin; however, the 200-μm- and 400-μm-width channels contained a less-thick epidermis. The percentage of Ki67-positive cells for the 200-μm- and 400-μm-width channels both decreased at the 7-day time point and was statistically different from the 3 days, which could indicate that the epithelial thickness in these channels was at its maximum. To further support the proposed mechanism, as well as to further explain the trends observed, future studies will focus on collecting data at later time points to evaluate whether the epithelial thickness of the wider channels reaches similar thickness values as the 50-μm-width and 100-μm-width channels, epithelialized DED, and native tissue. Additionally, studies to characterize the expression of differentiation markers will help to understand the differentiation status of the cells located in the channels.

Epidermal keratinocyte interactions with the underlying matrix are critical for tissue organization and functionality. As mediators of cell surface interactions at the DEJ, evaluating the expression and localization of integrins, specifically β_1, on the surface of the cell can suggest renormalized keratinocyte adhesion.[48,49] Additionally, the amount and activation status of β_1 integrins on the cell surface have been used to distinguish the proliferative potential of keratinocytes as well as their commitment to terminal differentiation.

On the surface of the μDERMs, β_1 integrin staining was found pericellular, and differences between β_1 intensity levels were observed. These data suggest a heterogeneous population of basal keratinocytes, as seen in native skin, demonstrating a population of proliferative cells and cells that are committed to undergoing terminal differentiation. Interestingly, β_1-bright cells were found primarily in the channels of the μDERMs as well as in the rete ridges of epithelialized DED. This finding suggests that the μDERMs provide an environment for stem cell niche formation. To further evaluate this hypothesis, the transmembrane protein

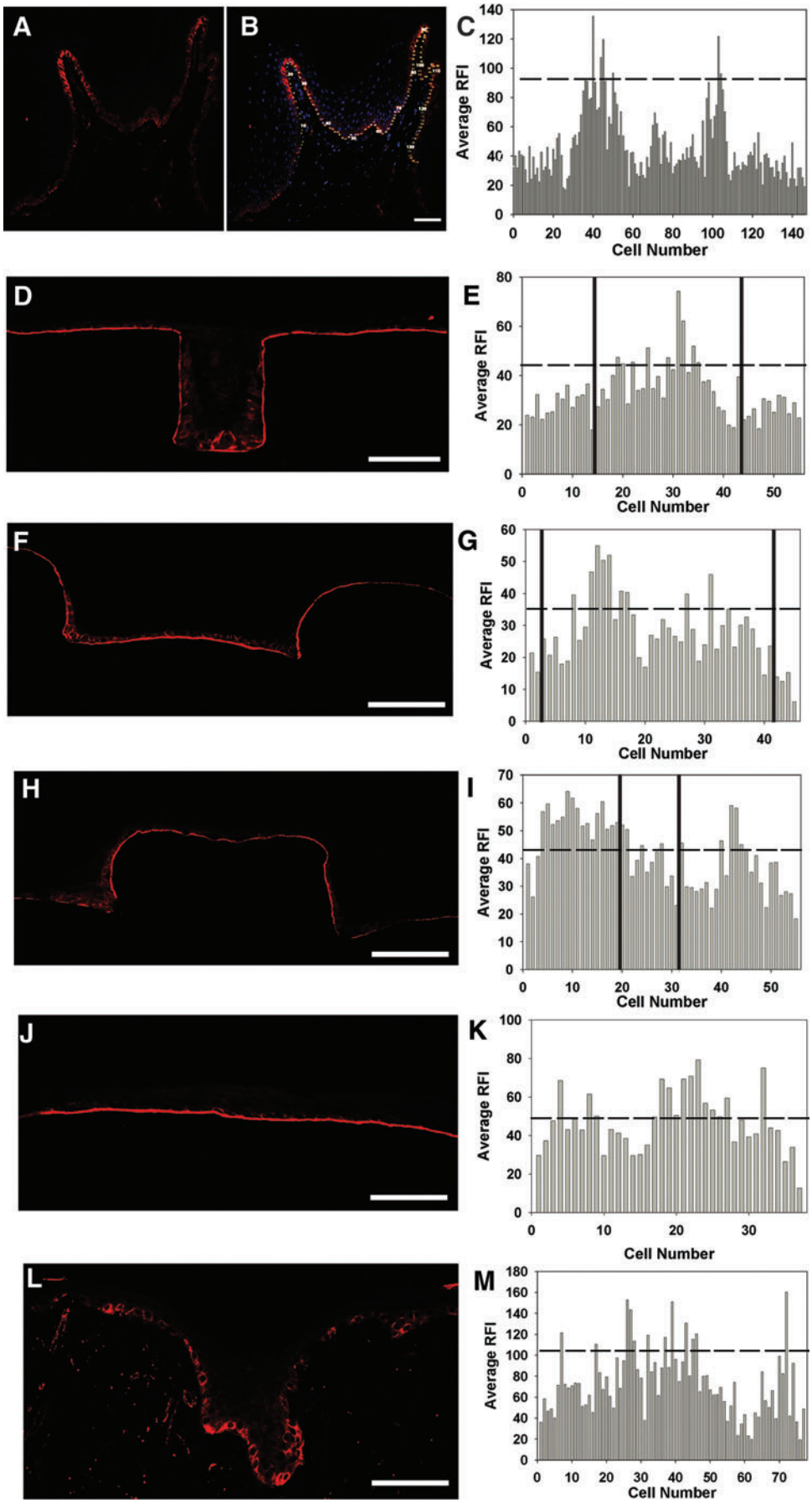

FIG. 8. β_1 integrin expression of basal keratinocytes on μDERMs, DED, and native foreskin tissue. To determine the localization of β_1-bright basal keratinocytes, immunohistochemistry coupled with digital image analyses was used. For each sample, β_1 expression was evaluated for each cell, and the RFI of each cell was plotted to determine the intensity levels. The dashed line in each plot represents the upper 1/3 intensity values indicative of β_1-bright cells. **(A)** is a representative image of β_1 expression of foreskin tissue, and **(B)** is a combination of β_1 expression and nuclear staining of the same sample. The numbers in **(B)** indicate the cell number that correlates with the plot in **(C)**. For each channel width, β_1 expression was evaluated, and the RFI was plotted. The solid vertical lines represent the edges of the channels. **(D)** and **(E)** represent 100-μm-width channels; **(F)** and **(G)** represent 400-μm-width channels; **(H)** and **(I)** represent the corners of 400-μm-width channels, **(J)** and **(K)** are flat control regions of the μDERMs, and **(L)** and **(M)** represent epithelialized DED. Scale bars represent 100 μm for all images. Color images available online at www.liebertpub.com/tea

LR1G1, recently identified as a strong marker for epidermal stem cell localization,[50,51] cytokeratin 19,[52,53] cytokeratin 15,[52] and p63[52,54] should be analyzed concurrently with β_1 to evaluate the ability of the formation of stem cell niches and regenerative capacity of μDERMs.

β_1 integrin expression on μDERMs suggests a robust interaction between basal keratinocytes and the underlying dermal matrix; however, to fully assess whether this interaction can sustain keratinocyte growth and differentiation, the evaluation of a basement membrane structure is required. The deposition and assembly of the basement membrane occurs with the normalization of epithelial growth, morphogenesis, and differentiation, and are mediated by epithelial and mesenchymal factors.[55–57] Incorporation of dermal fibroblasts into the μDERMs is currently being undertaken to evaluate the formation of a structured basement membrane and the complete microenvironment found at the DEJ.

Overall, this study has focused on developing a matrix (μDERM) that provides the 3D features found at the DEJ and demonstrates the effect of the native features on epithelialization, proliferation, and keratinocyte localization. The data demonstrate that channels with the narrowest openings had enhanced epithelialization and were comparable to cultures on DED. These small channels mimic rete ridges found in areas of the body that undergo excessive friction, and incorporating these features may improve not only epithelialization rates but also the cohesion between the dermis and the epidermis after a mechanical stress. The data gathered from this study also suggest the formation of a stem cell niche that provides a protective environment from external insults and warrants further evaluation of epithelial stem cell markers to further support this claim.

Acknowledgments

This research was funded by the NIH (EB-005645). The authors wish to thank Dr. Mehmet Toner and Octavio Hurtado at the BioElectroMechanical Systems (BioMEMS) Resource Center, Massachusetts General Hospital, Boston, MA (NIH Grant: P41 EB02503 [MT]), for their assistance with the microfabrication processes. The authors would also like to thank the Department of Obstetrics and Gynecology at UMMS (Worcester, MA) for providing us with neonatal foreskins for keratinocyte isolations and Russell Kronengold, Ph.D., at the Kensey Nash Corporation (Exton, PA), for his generous donations of SEMED-S collagen.

Disclosure Statement

No competing financial interests exist.

References

1. Yannas, I.V., Orgill, D.P., and Burke, J.F. Template for skin regeneration. Plast Reconstr Surg **127 Suppl 1,** 60S, 2011.
2. Clark, R.A., Ghosh, K., and Tonnesen, M.G., Tissue engineering for cutaneous wounds. J Invest Dermatol **127,** 1018, 2007.
3. Ehrenreich, M., and Ruszczak, Z. Update on tissue-engineered biological dressings. Tissue Eng **12,** 2407, 2006.
4. Supp, D.M., and Boyce, S.T. Engineered skin substitutes: practices and potentials. Clin Dermatol **23,** 403, 2005.
5. Shevchenko, R.V., James, S.L., and James, S.E. A review of tissue-engineered skin bioconstructs available for skin reconstruction. J R Soc Interface **7,** 229, 2010.
6. Boyce, S.T. Cultures skin substitutes: a review. Tissue Eng **2,** 255, 1996.
7. Boyce, S.T., *et al.* Comparative assessment of cultured skin substitutes and native skin autograft for treatment of full-thickness burns. Ann Surg **222,** 743, 1995
8. Parenteau, N., *et al.* Biological and physical factors influencing the successful engraftment of a cultured skin substitute. Biotech Bioeng **52**, 3, 1996.
9. Sheridan, R.L., and Tompkins, R.G. Skin substitutes in burns. Burns **25,** 97, 1999.
10. Lazic, T., and Falanga, V. Bioengineered skin constructs and their use in wound healing. Plast Reconstr Surg **127 Suppl 1,** 75S, 2011.
11. Bottcher-Haberzeth, S., Biedermann, T., and Reichmann, E. Tissue engineering of skin. Burns **36,** 450, 2010.
12. Odland, G. The morphology of the attachment between the dermis and the epidermis. Anat Record **108,** 399, 1950.
13. Fawcet, D.W., and Jensh, R.P. Concise Histology. New York, NY: Chapman and Hall, 1997.
14. Watt, F.M., and Hertle, M.D. Keratinocyte integrins. In Leigh, I. Birgitte, L., and Watt, F., eds. The Keratinocyte Handbook. New York, NY: Press Syndicate of the University of Cambridge, 1994.
15. Hotchin, N., Gandarillas, A., and Watt, F. Regulation of cell surface beta 1 integrin levels during keratinocyte terminal differentiation. J Cell Biol **128,** 1209, 1995.
16. Hotchin, N., and Watt, F. Transcriptional and post-translational regulation of beta 1 integrin expression during keratinocyte terminal differentiation. J Biol Chem **267,** 14852, 1992.
17. Watt, F.M., *et al.* Regulation of keratinocyte terminal differentiation by integrin-extracellular matrix interactions. J Cell Sci **106 (Pt 1),** 175, 1993.
18. Hotchin, K.J., and Watt, F.M. Functional down regulation of alpha5beta1 integrin in keratinocytes is reversible but commitment to terminal differentiation is not. J Cell Sci **106,** 1131, 1994.
19. Nicholson, L.J., and Watt, F.M. Decreased expression of fibronectin and the alpha 5 beta 1 integrin during terminal differentiation of human keratinocytes. J Cell Sci **98 (Pt 2),** 225, 1991.
20. Levy, L., *et al.* beta1 integrins regulate keratinocyte adhesion and differentiation by distinct mechanisms. Mol Biol Cell **11,** 453, 2000.
21. Jensen, U.B., Lowell, S., and Watt, F.M. The spatial relationship between stem cells and their progeny in the basal layer of human epidermis: a new view based on whole-mount labelling and lineage analysis. Development **126,** 2409, 1999.
22. Jones, P.H., Harper, S., and Watt, F.M. Stem cell patterning and fate in human epidermis. Cell **80,** 83, 1995.
23. Jones, P.H., and Watt, F.M. Separation of human epidermal stem cells from transit amplifying cells on the basis of differences in integrin function and expression. Cell **73,** 713, 1993.
24. Lavker, R.M., and Sun, T.T. Heterogeneity in epidermal basal keratinocytes: morphological and functional correlations. Science **215,** 1239, 1982
25. Lavker, R.M., and Sun, T.T. Epidermal stem cells. J Invest Dermatol **81(1 Suppl),** 121s, 1983.
26. Downing, B.R., *et al.* The influence of microtextured basal lamina analog topography on keratinocyte function and epidermal organization. J Biomed Mater Res A **72,** 47, 2005.

27. Cornwell, K.G., Downing, B.R., and Pins, G.D. Characterizing fibroblast migration on discrete collagen threads for applications in tissue regeneration. J Biomed Mater Res A **71,** 55, 2004.
28. Elsdale, T., and Bard, J. Collagen substrata for studies on cell behavior. J Cell Biol **54,** 626, 1972.
29. Bush, K.A., and Pins, G.D. Carbodiimide conjugation of fibronectin on collagen basal lamina analogs enhances cellular binding domains and epithelialization. Tissue Eng **16,** 829, 2010.
30. Bush, K.A., *et al.* Conjugation of extracellular matrix proteins to basal lamina analogs enhances keratinocyte attachment. J Biomed Mater Res A **80,** 444, 2007.
31. Olde Damink, L.H., *et al.* Cross-linking of dermal sheep collagen using a water-soluble carbodiimide. Biomaterials **17,** 765, 1996.
32. Pins, G.D., Toner, M., and Morgan, J.R. Microfabrication of an analog of the basal lamina: biocompatible membranes with complex topographies. Faseb J **14,** 593, 2000.
33. Boyce, S.T., and Williams, M.L., Lipid supplemented medium induces lamellar bodies and precursors of barrier lipids in cultured analogues of human skin. J Invest Dermatol **101,** 180, 1993.
34. Moles, J.P., and Watt, F.M. The epidermal stem cell compartment: variation in expression levels of E-cadherin and catenins within the basal layer of human epidermis. J Histochem Cytochem **45,** 867, 1997.
35. Bosca, A.R., *et al.* Epithelial differentiation of human skin equivalents after grafting onto nude mice. J Invest Dermatol **91,** 136, 1988.
36. Boyce, S.T., *et al.* Skin anatomy and antigen expression after burn wound closure with composite grafts of cultured skin cells and biopolymers. Plast Reconstr Surg **91,** 632, 1993.
37. Cooper, M., and Hansbrough, J.F. Use of a composite skin gaft composed of cultured human keratinocytes and fibroblasts and a collagen-GAG matrix to cover full-thickness wounds on athymic mice. Surgery **109,** 198, 1991.
38. Cooper, M.L., *et al.* Direct comparison of a cultured composite skin substitute containing human keratinocytes and fibroblasts to an epidermal sheet graft containing human keratinocytes on athymic mice. J Invest Dermatol **101,** 811, 1993.
39. Hansbrough, J.F., *et al.* Composite grafts of human keratinocytes grown on a polyglactin mesh-cultured fibroblast dermal substitute function as a bilayer skin replacement in full-thickness wounds on athymic mice. J Burn Care Rehabil **14,** 485, 1993.
40. Medalie, D.A., *et al.* Differences in dermal analogs influence subsequent pigmentation, epidermal differentiation, basement membrane, and rete ridge formation of transplanted composite skin grafts. Transplantation **64,** 454, 1997.
41. Holbrook, K.A. Ultrastructure of the epidermis. In: Leigh, I. Lane, B., and Watt, F.M. eds. The Keratinocyte Handbook. New York: Cambridge University Press, 1994, pp. 3–39.
42. Yuspa, S.H., *et al.* Expression of murine epidermal differentiation markers is tightly regulated by restricted extracellular calcium concentrations in vitro. J Cell Biol **109,** 1207, 1989.
43. Pillai, S., *et al.* Calcium regulation of growth and differentiation of normal human keratinocytes: modulation of differentiation competence by stages of growth and extracellular calcium. J Cell Physiol **143,** 294, 1990.
44. Poumay, Y., and Pittelkow, M.R. Cell density and culture factors regulate keratinocyte commitment to differentiation and expression of suprabasal K1/K10 keratins. J Invest Dermatol **104,** 271, 1995.
45. Kolly, C., Suter, M.M., and Muller, E.J. Proliferation, cell cycle exit, and onset of terminal differentiation in cultured keratinocytes: pre-programmed pathways in control of C-Myc and Notch1 prevail over extracellular calcium signals. J Invest Dermatol **124,** 1014, 2005.
46. Clark, R. Wound repair, overview and general considerations. In: Clark, R. ed. The Molecular and Cellular Biology of Wound Repair (Second Edition). New York: Plenum Press, 1995, pp. 3–44.
47. Watt, F.M., Lo Celso, C., and Silva-Vargas, V. Epidermal stem cells: an update. Curr Opin Genet Dev **16,** 518, 2006.
48. Stark, H.J., *et al.* Authentic fibroblast matrix in dermal equivalents normalises epidermal histogenesis and dermoepidermal junction in organotypic co-culture. Eur J Cell Biol **83,** 631, 2004.
49. Boehnke, K., *et al.* Effects of fibroblasts and microenvironment on epidermal regeneration and tissue function in long-term skin equivalents. Eur J Cell Biol **86,** 731, 2007.
50. Jensen, K.B., Driskell, R.R., and Watt, F.M. Assaying proliferation and differentiation capacity of stem cells using disaggregated adult mouse epidermis. Nat Protoc **5,** 898, 2010.
51. Jensen, K.B., and Watt, F.M. Single-cell expression profiling of human epidermal stem and transit-amplifying cells: Lrig1 is a regulator of stem cell quiescence. Proc Natl Acad Sci U S A **103,** 11958, 2006.
52. Abbas, O., *et al.* Stem cell markers (cytokeratin 15, cytokeratin 19 and p63) in in situ and invasive cutaneous epithelial lesions. Mod Pathol **24,** 90, 2011.
53. Michel, M., *et al.* Keratin 19 as a biochemical marker of skin stem cells in vivo and in vitro: keratin 19 expressing cells are differentially localized in function of anatomic sites, and their number varies with donor age and culture stage. J Cell Sci **109 (Pt 5),** 1017, 1996.
54. Pellegrini, G., *et al.* p63 identifies keratinocyte stem cells. Proc Natl Acad Sci U S A **98,** 3156, 2001.
55. Andriani, F., *et al.* Analysis of microenvironmental factors contributing to basement membrane assembly and normalized epidermal phenotype. J Invest Dermatol **120,** 923, 2003.
56. Segal, N., *et al.* The basement membrane microenvironment directs the normalization and survival of bioengineered human skin equivalents. Matrix Biol **27,** 163, 2008.
57. El Ghalbzouri, A., *et al.* Basement membrane reconstruction in human skin equivalents is regulated by fibroblasts and/or exogenously activated keratinocytes. J Invest Dermatol **124,** 79, 2005.

Address correspondence to:
George D. Pins, Ph.D.
Department of Biomedical Engineering
Worcester Polytechnic Institute
100 Institute Road
Worcester, MA 01609

E-mail: gpins@wpi.edu

Received: August 24, 2011
Accepted: May 10, 2012
Online Publication Date: July 30, 2012